RSC Advances

PAPER

View Article Online
View Journal | View Issue

Cite this: *RSC Adv.*, 2025, **15**, 5214

Exploring the efficient antimicrobial applications of a novel supramolecular Hg(II)-metallogel derived from succinic acid acting as a low molecular weight gelator

Subhendu Dhibar,†*[a] Suchetana Pal,†[b] Sangita Some,[a] Kripasindhu Karmakar,[a] Ratnakar Saha,[c] Subham Bhattacharjee,[d] Dimpal Kumari,[e] Aiswarya Mohan,[f] Timothy O. Ajiboye,[g] Soumya Jyoti Ray,[e] Sanjay Roy,[h] Somasri Dam*[b] and Bidyut Saha*[a]

A novel supramolecular metallogel, termed Hg-SA, was synthesized using succinic acid (SA) as a low molecular weight gelator in a DMF solvent under standard conditions. The mechanical properties of the Hg-SA metallogel were evaluated through rheological tests, specifically focusing on the angular frequency and strain sweep measurements. Field emission scanning electron microscopy (FESEM) results revealed the rod-like network structure of Hg-SA, while energy dispersive X-ray (EDX) elemental mapping confirmed its composition. Fourier transform infrared (FT-IR) spectroscopy provided insights into the formation mechanism of the synthesized Hg-SA metallogel. The antimicrobial activity of the metallogel was tested against Gram-positive bacteria *Bacillus subtilis* and *Staphylococcus epidermidis* as well as Gram-negative bacteria *Escherichia coli* and *Pseudomonas aeruginosa*, revealing its significant antibacterial potency. Thus, this study highlights the antimicrobial effects of Hg(II)-based succinic acid-mediated metallogels against Gram-positive and Gram-negative bacteria.

Received 5th December 2024
Accepted 30th January 2025

DOI: 10.1039/d4ra08575b

rsc.li/rsc-advances

1. Introduction

Gels typically include an elastic, three-dimensional, cross-linked network that traps a liquid.[1] The gelator molecule traps solvent molecules within this network, leading to gel formation.[2,3] The inversion vial test is a common method to identify the gel formation when the gel is not disturbed by gravity.[1–4] Low molecular weight gelators (LMWGs), with molecular masses below 3000, serve as the building blocks that immobilize solvents through various interactions, such as hydrophobic and hydrophilic interactions, van der Waals forces, hydrogen bonding, ion–dipole, dipole–dipole, and π···π stacking, creating the supramolecular gel.[1,2,5,6] Numerous LMWGs,[1] including dicarboxylic acids,[1] sugars,[7,8] peptides,[9] amino acids,[2] urea derivatives,[4] bile acids,[5] cholesterol,[7] carbohydrates,[1] saccharides,[7] amides,[1] and alkenes,[5] have been studied. Solvents are also crucial in gel formation[5] as their polarity and viscosity can alter the gel morphology. Common solvents used include DMF,[1] water,[4] acetone,[10] alcohols,[2] hexane,[11] 1,2-dichlorobenzene,[5] toluene,[3] and acetonitrile.[12] Owing to the weak non-covalent interactions, LMWGs are also capable of reversible gel-to-sol phase transition with changes in electrolytes, pH, temperature, and external mechanical factors.[13] This adaptability makes these gels appealing for various applications, including sensors,[14] drug delivery,[15a] and water remediation.[15b] They are particularly promising in controlled release systems owing to their ability to encapsulate and release chemicals within the gel matrix.[16]

Supramolecular metallogels, a subset of these gels, are formed when metal ions or metal complexes with organic ligands (LMWGs) self-assemble into complex three-dimensional networks.[17] The unique properties of supramolecular metallogels can be finely tuned by selecting specific metal ions and ligands and manipulating their environment.[18]

[a]*Colloid Chemistry Laboratory, Department of Chemistry, The University of Burdwan, Golapbag, Burdwan, 713104, West Bengal, India. E-mail: sdhibar@scholar.buruniv.ac.in; bsaha@chem.buruniv.ac.in; Tel: +91 7001575909; +91 9476341691*

[b]*Department of Microbiology, The University of Burdwan, Burdwan, 713104, West Bengal, India. E-mail: sdam@microbio.buruniv.ac.in*

[c]*National Institute of Science Education and Research (NISER), Bhubaneswar, Odisha, 752050, India*

[d]*Department of Chemistry, Kazi Nazrul University, Asansol, 713303, West Bengal, India*

[e]*Department of Physics, Indian Institute of Technology Patna, Bihar, 801106, India*

[f]*Laboratory for Molecular Photonics and Electronics (LAMP), Department of Physics, National Institute of Technology Calicut, Calicut, 673603, Kerala, India*

[g]*Department of Chemistry, University of the Free State, Bloemfontein, 9301, South Africa*

[h]*Department of Chemistry, School of Science, Netaji Subhas Open University, Kalyani Regional Centre, Kolkata, 741251, India*

† SD and SP should be treated as joint first authors.

In this regard, transition metal-based metallogels have attracted significant attention owing to their cost-effectiveness, accessibility, and enhanced ability to coordinate with organic ligands. Metal ions like Ni(II),[12] Cu(II),[2] Co(II),[1a,19] Zn(II),[10,20] Fe(II/III),[4b,21] Cd(II),[6,18] Hg(II),[18] and Mn(II)[22] have been used to create a wide range of metallogels, demonstrating their flexibility and potential applications. Dicarboxylic acids,[1,6,18] in particular, enhance interactions with transition metals, facilitating gelation. Succinic acid (SA), an intermediate in the citric acid cycle, also functions as an antioxidant and antibacterial agent, and it is widely used in food and drinks as a flavoring agent and preservative.[23,24] It enables the synthesis of high aspect ratio functional supramolecular metallogels, expanding their potential applications. Recent research has shown the antibacterial activity of Hg(II)-based systems, particularly in biological contexts, showcasing promising directions in metallogel research. Our research explores the metallo-gelation potential of succinic acid using Hg(II) in *N*,*N*-dimethylformamide solvent. We conducted rheological studies to assess the mechanical properties and performed morphological analysis and elemental characterization using FESEM and energy-dispersive X-ray studies. The emergence of drug-resistant organisms due to traditional antibiotics has necessitated the urgent discovery of new antimicrobial agents. Metallogel moieties offer intriguing potential for inhibiting bacterial growth. Metallogels can compromise the integrity of bacterial cell membranes, leading to the efflux of intracellular components.[25] Bacterial DNA, proteins, and lipids are vulnerable to damage caused by reactive oxygen species (ROS) generated by some metallogels.[26] Inexpensive, naturally derived polyphenols combined with metal ions form gels that have been shown to heal infected wounds effectively.[27] The combination of peptide nanofibers and silver nanoparticles within a gel matrix offers antimicrobial benefits.[26] Ni(II) and Zn(II)-based gel materials exhibit antimicrobial activity against a range of human-infecting microorganisms.[28] A metallogel formed from the combination of suberic acid with nickel, zinc, or cadmium shows promise in combating bacterial pathogens.[29] However, there is evidence that Hg is toxic to cells. Hg induces significant cytotoxicity in human liver cells.[30] Hg toxicity causes membrane disintegration in the human peripheral immune cells.[31] Our research underscores the potential of Hg(II)-based metallogels with succinic acid as novel treatments for microbial infections. The novelty of this work lies in the exploration of Hg(II)-based metallogels with succinic acid as a gelator, demonstrating potent antimicrobial properties against both Gram-positive and Gram-negative bacteria. Unlike other metallogels, our study emphasizes the unique role of Hg(II) in the gelation process and highlights the promising potential of Hg(II)-based metallogels as novel treatments for microbial infections.[2,32]

2. Experimental

2.1 Reagents

Mercury(II) acetate (≥98.0%), succinic acid, and DMF were sourced from Merck Chemical Company and used without further purification. Dry DMF was consistently employed throughout the experiments. Tryptone, D-(+)-glucose anhydrous, and yeast extract powder were obtained from Himedia.

2.2 Apparatus and measurements

The metallogel synthesis was performed using a Phoenix Digital Ultrasonic Cleaner PHUC-150. Rheological analysis was conducted using a cone-plate rheometer from TA instruments. Field emission scanning electron microscopy (FESEM) was carried out using a Carl Zeiss SUPRA 55VP FESEM instrument, and energy-dispersive X-ray spectroscopy (EDX) was conducted in the scanning mode using the ZEISS EVO 18 apparatus. Topography analysis was performed with an atomic force microscope (Agilent Technology 5500) in noncontact mode, utilizing a silicon tip. The FT-IR spectrum of the metallogel was analyzed using a JASCO FTIR 4700 spectrometer.

2.3 Preparation of Hg(II)-metallogel (Hg-SA)

The stable white Hg-SA metallogel was prepared by rapidly mixing 1 mL of a DMF solution of mercury acetate (1 mmol, 0.318 g) with 1 mL of a DMF solution of succinic acid (2 mmol, 0.236 g), followed by continuous ultrasonication in a water bath for ten minutes (Fig. 1). This process induces the formation of a supramolecular network *via* non-covalent interactions between the mercury metal ions and succinic acid in the DMF solvent, resulting in a stable three-dimensional structure. Ultrasonication accelerates the gelation process by enhancing the mixing and assembly of these components (Fig. 1). We determined the minimal critical gelation concentration (MGC) of the Hg-SA metallogel. To ascertain the MGC of Hg-SA, we varied the concentrations of the $Hg(CH_3COO)_2$ salt and succinic acid (10–554 mg mL^{-1}). A stable Hg-TA metallogel was formed at a concentration of 554 mg mL^{-1} of Hg(II)-acetate salt and succinic acid in DMF solvent.

2.4 Antimicrobial activity of the Hg-SA metallogel

The antimicrobial activity of Hg-SA was determined using a zone of inhibition assay. The metallogel was suspended in deionized water (Merck, Millipore, France) at a concentration of 100 mg mL^{-1}. The antimicrobial activity was studied against four pathogenic bacterial strains: two Gram-negative *Escherichia coli* (*E. coli*), *Pseudomonas aeruginosa* (*P. aeruginosa*) and two Gram-positive *Bacillus subtilis* (*B. subtilis*), *Staphylococcus epidermidis* (*S. epidermidis*). Streptomycin was used as a positive

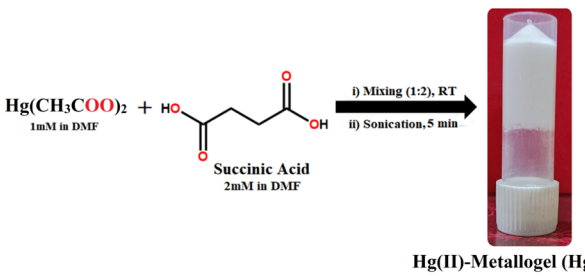

Fig. 1 Schematic of the synthetic route of the Hg(II)-metallogel (Hg-SA).

control. Its broad-spectrum activity against both Gram-positive and Gram-negative bacteria, including rare strains, makes it reliable for demonstrating antibiotic efficacy in a zone of inhibition assay. Each bacterial inoculum was evenly spread using a sterile cotton swab on TGE (tryptone, glucose, yeast extract, all at 1%; pH 6.5) agar plates. Agar plates were spotted with 10 μL of each metallogel suspension. The plates were incubated at 37 °C for 24 hours and inspected for distinct inhibitory zones. The experiment was carried out in triplicate.

3. Results and discussion

3.1 Rheological analysis

The semi-solid nature of the Hg-SA metallogel was characterized using rheological analysis, focusing on angular frequency and strain-sweep measurements. The storage modulus (G') was found to be significantly higher than the loss modulus (G''), confirming the material's gel-like properties. Rheological data revealed that the Hg-SA metallogel maintained a higher storage modulus ($G' > 10^2$ Pa) compared to the loss modulus (G'') at a specific concentration of $Hg(CH_3COO)_2$ and succinic acid ([Hg(II)] = 554 mg mL^{-1}) (Fig. 2a). This indicates its semi-solid nature and substantial tolerance. Strain-sweep measurements, conducted at a constant frequency of 6.283 rad s^{-1}, showed that G' exceeded G'' up to a critical strain of 0.03392%, indicating the point at which the gel begins to break down. These results are illustrated in Fig. 2b.

3.2 Microstructural study

Field emission scanning electron microscopy (FESEM) of the Hg-SA metallogel revealed a rod-like hierarchical network structure (Fig. 3a and b). This microstructural arrangement was formed by combining $Hg(OAc)_2$ and succinic acid in a DMF medium, facilitated by constant sonication. The structural integrity of the Hg-SA metallogel's network is likely due to the predominant supramolecular interactions. Elemental composition mapping by EDX (Fig. 3c–g) confirmed the presence of carbon (C), nitrogen (N), oxygen (O), and mercury (Hg) elements from $Hg(OAc)_2$, succinic acid, and DMF molecules, which are essential for the formation of the Hg-SA metallogel network.

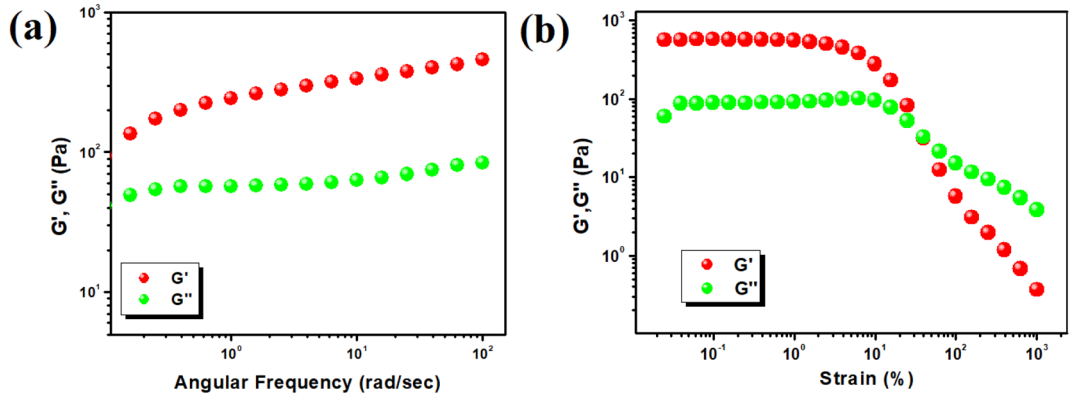

Fig. 2 Rheological analysis of the Hg-SA metallogel: (a) graph illustrating the storage modulus (G') and loss modulus (G'') as functions of angular frequency; (b) strain-sweep analysis of the Hg-SA metallogel conducted at a constant frequency of 6.283 rad s^{-1}.

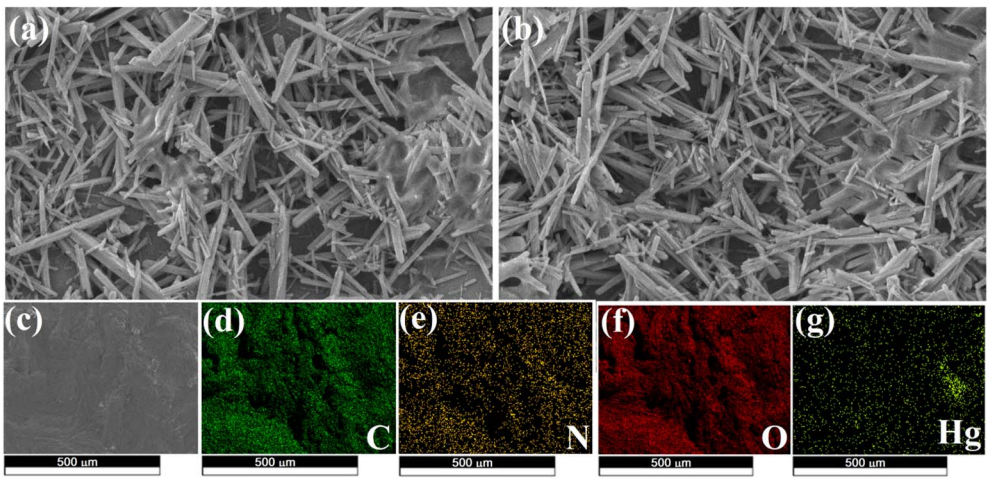

Fig. 3 FESEM images (a) and (b) highlighting the microstructural features of the Hg-SA metallogel. Elemental mapping images (c)–(g) displaying the spatial distribution of key elements, including carbon (C), nitrogen (N), oxygen (O), and mercury (Hg), within the sample.

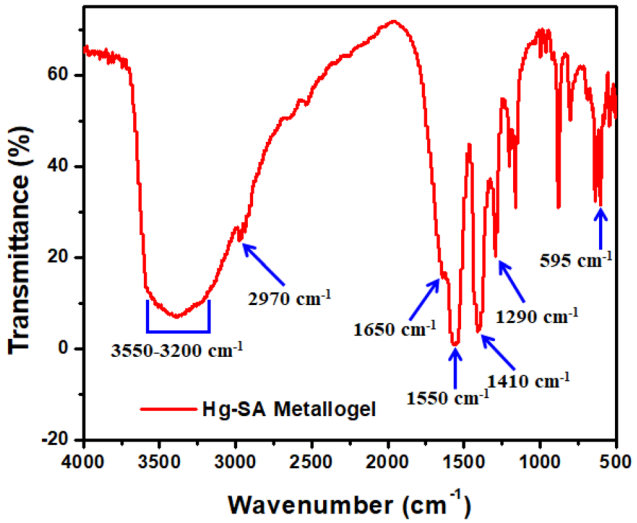

Fig. 4 FT-IR spectra of the xerogel form of the Hg-SA metallogel.

3.3 FT-IR analysis of the Hg-SA metallogel

To characterize the synthesized Hg-SA metallogel, Fourier transform infrared (FT-IR) spectroscopy was performed due to its sensitivity to different functional groups. The FT-IR spectra of the xerogel forms of Hg-SA metallogel reveal the supramolecular interactions between succinic acid and the Hg(II) sources, which are responsible for the formation of the metallogel (Fig. 4). In the Hg-TA metallogel, significant spectral absorption bands include the O–H stretching of hydroxyl groups, visible as a broad peak at 3550–3200 cm^{-1} (Fig. 4). The vibrational mode at 2970 cm^{-1} corresponds to the symmetric C–H bonds. The carboxyl C=O stretching in the carboxyl group is associated with peaks at 1650 cm^{-1}. Vibrational modes associated with peaks at 1550 cm^{-1}, 1410 cm^{-1}, and 1290 cm^{-1} represent N–O stretching, C–N stretching, and C–O stretching, respectively. Furthermore, a peak at 595 cm^{-1} confirms the presence of the Hg–O bond, strengthening the connection between succinic acid and DMF-soluble mercury acetate.

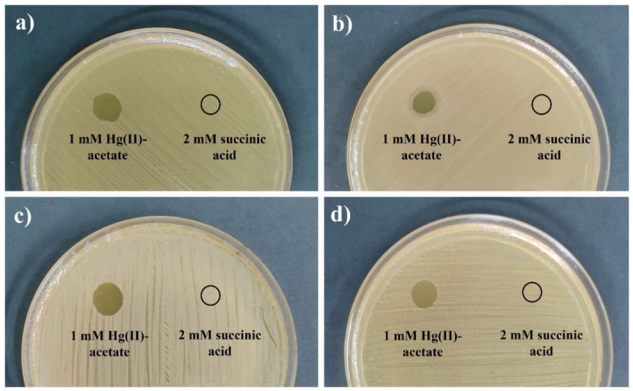

Fig. 5 Zone of inhibition observed in (a) *E. coli*, (b) *P. aeruginosa*, (c) *B. subtilis* and (d) *S. epidermidis* in places spotted with 1 mM Hg(II)-acetate. 2 mM succinic acid did not produce any inhibitory zones.

3.4 Inhibiting activity for pathogens

A high concentration of an antimicrobial substance inhibits bacterial development, leading to a circular region without bacterial colonies, termed the zone of inhibition. Synthesized derivatives are promising when they match the control antibiotic's effectiveness. The result indicates that Hg-SA exhibits potent antimicrobial activity against Gram-negative *E. coli*, *P. aeruginosa* and Gram-positive *B. subtilis*, *S. epidermidis* (Fig. 6 and Table 1). The absence of an inhibition zone in plates spotted with 2 mM succinic acid indicated that the antimicrobial activity observed with Hg-SA was not attributable to the antimicrobial properties of succinic acid. However, given its recognized antimicrobial properties, 1 mM Hg(II)-acetate showed inhibitory zones against all four bacterial strains (zone of inhibition: 10 mm against *E. coli*, 10 mm against *P. aeruginosa*, 11 mm against *B. subtilis*, 10 mm against *S. epidermidis*) (Fig. 5). But diameters of inhibitory zones are significantly higher post-gelation (Fig. 6). It can be concluded that sonication and gelation enhanced the antimicrobial activity, indicating a strong connection between gel formation and increased antimicrobial effectiveness.

Table 1 Antimicrobial activity of the Hg-SA metallogel[a]

Bacterial strain (s)	Zone of inhibition (mm in diameter) against streptomycin
E. coli	20.5 ± 0.5
P. aeruginosa	20.16 ± 0.28
B. subtilis	20.33 ± 0.57
S. epidermidis	13.16 ± 0.28

Metallogel	Bacterial strain (s)	Volume of metallogel given (μL)	Concentration of metallogel (mg mL^{-1})	Zone of inhibition (mm in diameter)
Hg-SA	*E. coli*	10	100	22.83 ± 0.28
	P. aeruginosa	10	100	27.33 ± 0.57
	B. subtilis	10	100	23.53 ± 0.50
	S. epidermidis	10	100	20.16 ± 0.5

[a] ±Standard deviation.

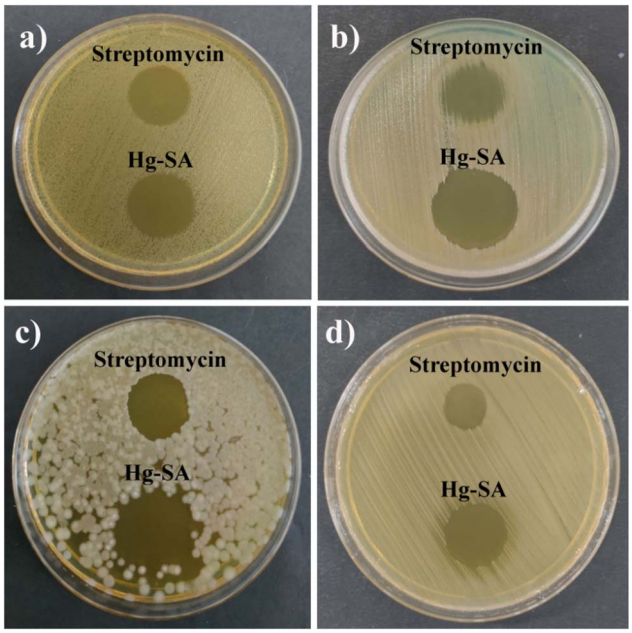

Fig. 6 Anti-microbial activity of Hg-SA against four pathogenic strains (a) *E. coli*, (b) *P. aeruginosa*, (c) *B. subtilis* and (d) *S. epidermidis*. The presence of clear areas signifies that bacterial growth was successfully prevented. The metallogel gradually spread throughout the agar medium and suppressed the bacterial growth.

The inherent toxicity of mercury, particularly in its ionic form (Hg^{2+}), is a well-documented challenge. To address these issues, our study focuses on designing the Hg-SA metallogel as a controlled-release system, where the release of mercury ions is regulated by the molecular interactions within the gel network. The gelation process, facilitated by the coordination between Hg(II) and succinic acid, not only stabilizes the mercury ions but also reduces their immediate bioavailability. This mechanism allows for a sustained and localized antimicrobial effect while minimizing systemic toxicity.

Additionally, the use of metallogels provides a distinct advantage in that the material can be applied in a site-specific manner, further reducing the likelihood of off-target effects. The Hg(II)-based metallogel should be used only where systemic exposure is negligible. For instance, in topical applications or coatings, the metallogel can deliver its antimicrobial activity precisely where it is needed, avoiding unnecessary exposure to the surrounding healthy tissues. Unlike systemic treatments, which are taken orally or injected and affect the entire body, topical treatments target only the area where they are applied. Gels are one of the common forms of topical treatments used for dermatological issues. In our study, we have used four bacterial strains, among which two (*P. aeruginosa* and *S. epidermidis*) can cause skin infections in addition to other manifestations.[33,34] In the antimicrobial activity assay, the metallogel showed significant inhibitory activity against these two pathogens. Considering the potential toxicities of Hg, it is essential to focus on controlled release and localized action when treating microbial infections.

Moreover, the concentration of Hg(II) in the metallogel is kept deliberately low (1 mM in this study), balancing efficacy and safety. To evaluate the viability of Hg(II)-based metallogels for real-world applications, future studies must systematically investigate their cytotoxicity profiles using *in vitro* and *in vivo* models. Such studies would provide comprehensive insights into the safety margins and potential therapeutic indices of these materials. In addition, efforts can be directed toward modifying the gel composition to further fine-tune the release kinetics of Hg(II) ions or incorporating chelating agents that neutralize excess mercury after exerting its antimicrobial effects. While we acknowledge the concerns surrounding the use of mercury-based materials, we believe that the novel design and controlled functionality of the Hg-SA metallogel present a promising approach for addressing microbial infections, particularly in cases where conventional treatments fail due to antibiotic resistance.

4. Conclusions

In conclusion, this study successfully synthesized an innovative Hg(II)-based metallogel through a straightforward process involving the direct mixing of mercury acetate and succinic acid solutions, followed by ultrasonication at room temperature. The metallogels demonstrated distinct morphological patterns, confirmed by FESEM microstructural analysis and exhibited robust mechanical stability as shown by rheological tests. FT-IR spectroscopy provided insights into the potential intermolecular interactions within the gel structures. Most notably, the antibacterial assays highlighted the significant potential of these metallogels as powerful inhibitors of harmful and lethal bacteria. These findings suggest that Hg(II)-metallogels hold substantial promise for diverse applications, particularly in the biomedical and pharmaceutical sectors, where antimicrobial properties are crucial. The synthesis protocol developed here paves the way for future exploration, with the potential for fine-tuning the material for specific applications. Interdisciplinary collaborations could further enhance their integration into practical solutions for healthcare, environmental protection, and advanced materials science. This work offers a transformative pathway for scientific and technological advancements with broad implications for addressing critical societal challenges.

Data availability

The data supporting the findings of this study are available within the paper. If any raw data files are needed in a different format, they are available from the corresponding author upon reasonable request.

Conflicts of interest

The authors declare no competing financial interests.

Acknowledgements

S. D. is grateful to the UGC, New Delhi, for awarding him Dr DS Kothari Postdoctoral Fellowship (Award letter number: No. F.4-

2/2006 (BSR)/CH/19-20/0224). S. P. acknowledges the University Grants Commission (UGC), Government of India, for Senior Research Fellowship (Award letter number: 16-6(DEC.2018)/2019(NET/CSIR)). S. B. thankfully acknowledges the DST Inspire Faculty Research Grant (Faculty Registration No. IFA18-CH304; DST/INSPIRE/04/2018/000329). T. O. A. gratefully acknowledges the University of the Free State, South Africa, for the Postdoctoral Funding.

References

1 (*a*) S. Dhibar, H. Dahiya, K. Karmakar, S. Kundu, S. Bhattacharjee, G. C. Nayak, P. Karmakar, G. D. Sharma and B. Saha, *J. Mol. Liq.*, 2023, **370**, 121020; (*b*) S. Dhibar, B. Pal, K. Karmakar, S. Kundu, S. Bhattacharjee, R. Sahoo, S. M. Rahaman, D. Dey, P. P. Ray and B. Saha, *ChemistrySelect*, 2023, **8**, e202204214; (*c*) S. Dhibar, S. K. Ojha, A. Mohan, S. P. C. Prabhakaran, S. Bhattacharjee, K. Karmakar, P. Karmakar, P. Predeep, A. K. Ojha and B. Saha, *New J. Chem.*, 2022, **46**, 17189–17200; (*d*) S. Dhibar, A. Dey, S. Majumdar, A. Dey, P. P. Ray and B. Dey, *Ind. Eng. Chem. Res.*, 2020, **59**, 5466–5473.

2 S. Dhibar, A. Dey, A. Dalal, S. Bhattacharjee, R. Sahu, R. Sahoo, A. Mondal, S. Mehebub Rahaman, S. Kundu and B. Saha, *J. Mol. Liq.*, 2023, **370**, 121021.

3 A. R. Hirst, B. Escuder, J. F. Miravet and D. K. Smith, *Angew. Chem., Int. Ed.*, 2008, **47**, 8002–8018.

4 (*a*) Y. Zhao, S. Song, X. Ren, J. Zhang, Q. Lin and Y. Zhao, *Chem. Rev.*, 2022, **122**, 5604–5640; (*b*) S. Dhibar, R. Jana, P. P. Ray and B. Dey, *J. Mol. Liq.*, 2019, **289**, 111126; (*c*) S. Dhibar, A. Dey, D. Ghosh, A. Mandal and B. Dey, *J. Mol. Liq.*, 2019, **276**, 184–193; (*d*) S. Dhibar, A. Dey, A. Dey, S. Majumdar, A. Mandal, P. P. Ray and B. Dey, *New J. Chem.*, 2019, **43**, 15691–15699; (*e*) D. Ghosh, S. Dhibar, A. Dey, S. Mukherjee, N. Joardar, S. P. Sinha Babu and B. Dey, *J. Mol. Liq.*, 2019, **280**, 1–12.

5 W.-L. Guan, K. M. Adam, M. Qiu, Y.-M. Zhang, H. Yao, T.-B. Wei and Q. Lin, *Supramol. Chem.*, 2020, **32**, 578–596.

6 S. Dhibar, S. Pal, K. Karmakar, S. A. Hafiz, S. Bhattacharjee, A. Roy, S. K. M. Rahaman, S. J. Ray, S. Dam and B. Saha, *RSC Adv.*, 2023, **13**, 32842–32849.

7 M.-O. M. Piepenbrock, G. O. Lloyd, N. Clarke and J. W. Steed, *Chem. Rev.*, 2010, **110**, 1960–2004.

8 A. Prathap and K. M. Sureshan, *Langmuir*, 2019, **35**, 6005–6014.

9 T.-A. Asoh and A. Kikuchi, *Chem. Commun.*, 2012, **48**, 10019.

10 K. Karmakar, A. Dey, S. Dhibar, R. Sahu, S. Bhattacharjee, P. Karmakar, P. Chatterjee, A. Mondal and B. Saha, *RSC Adv.*, 2023, **13**, 2561–2569.

11 L. Coppola, D. Coffetti and E. Crotti, *Constr. Build. Mater.*, 2018, **171**, 243–249.

12 P. Terech, M. Yan, M. Maréchal, G. Royal, J. Galvez and S. K. P. Velu, *Phys. Chem. Chem. Phys.*, 2013, **15**, 7338.

13 E. M. M. Ibrahim, L. H. Abdel-Rahman, A. M. Abu-Dief, A. Elshafaie, S. K. Hamdan and A. M. Ahmed, *Mater. Res. Bull.*, 2018, **107**, 492–497.

14 X. Cheng, J. Pan, Y. Zhao, M. Liao and H. Peng, *Adv. Energy Mater.*, 2018, **8**, 1702184.

15 (*a*) S. Dhibar, A. Roy, T. Sarkar, P. Das, K. Karmakar, S. Bhattacharjee, B. Mondal, P. Chatterjee, K. Sarkar, S. J. Ray and B. Saha, *Langmuir*, 2024, **40**, 179–192; (*b*) S. Dutta, A. Sinelshchikova, J. Andreo and S. Wuttke, *Nanoscale Horiz.*, 2024, **9**, 885–899; (*c*) S. Dutta, S. Fajal and S. K. Ghosh, *Acc. Chem. Res.*, 2024, **57**, 2546–2560.

16 A. Rajak and A. Das, *ACS Polymers Au*, 2022, **2**, 223–231.

17 X. Yang, H. Zhang, J. Zhao, Y. Liu, Z. Zhang, Y. Liu and X. Yan, *Chem. Eng. J.*, 2022, **450**, 138135.

18 S. Dhibar, A. Dey, S. Majumdar, D. Ghosh, A. Mandal, P. P. Ray and B. Dey, *Dalton Trans.*, 2018, **47**, 17412–17420.

19 S. Dhibar, S. Babu, K. Karmakar, A. Mohan, S. Bhattacharjee, S. M. Rahaman, G. C. Nayak, R. Saha, P. Predeep and B. Saha, *Chem. Phys. Lett.*, 2023, **829**, 140777.

20 (*a*) A. Roy, S. Dhibar, K. Karmakar, S. Bhattacharjee, B. Saha and S. J. Ray, *Sci. Rep.*, 2024, **14**, 13109; (*b*) A. Roy, S. Dhibar, K. Karmakar, S. Some, S. A. Hafiz, S. Bhattacharjee, B. Saha and S. J. Ray, *Mater. Adv.*, 2024, **5**, 3459–3471; (*c*) S. Dhibar, S. Babu, A. Mohan, G. K. Chandra, S. Bhattacharjee, K. Karmakar, P. Karmakar, S. M. Rahaman, P. Predeep and B. Saha, *J. Mol. Liq.*, 2023, **375**, 121348; (*d*) S. Dhibar, B. Pal, K. Karmakar, S. Roy, S. A. Hafiz, A. Roy, S. Bhattacharjee, S. J. Ray, P. P. Ray and B. Saha, *Nanoscale Adv.*, 2023, **5**, 6714–6723.

21 S. Dhibar, A. Dey, D. Ghosh, S. Majumdar, A. Dey, P. P. Ray and B. Dey, *ACS Omega*, 2020, **5**, 2680–2689.

22 S. Dhibar, A. Dey, A. Dey, S. Majumdar, D. Ghosh, P. P. Ray and B. Dey, *ACS Appl. Electron. Mater.*, 2019, **1**, 1899–1908.

23 I. Bechthold, K. Bretz, S. Kabasci, R. Kopitzky and A. Springer, *Chem. Eng. Technol.*, 2008, **31**, 647–654.

24 R. Kumar, B. Chandar and M. Parani, *Indian J. Med. Res.*, 2018, **147**, 97.

25 L. Qin, P. Wang, Y. Guo, C. Chen and M. Liu, *Adv. Sci.*, 2015, **2**, 1500134.

26 P. Bairagi, P. Ghosh, P. Roy and A. Banerjee, *ACS Appl. Nano Mater.*, 2023, **6**, 2299–2309.

27 H. T. P. Anh, C.-M. Huang and C.-J. Huang, *Sci. Rep.*, 2019, **9**, 11562.

28 G. Lepcha, B. Pal, S. Majumdar, K. T. Ahmed, I. Pal, S. R. Biswas, P. P. Ray and B. Dey, *Mater. Adv.*, 2023, **4**, 2595–2603.

29 G. Lepcha, S. Majumdar, B. Pal, K. T. Ahmed, I. Pal, B. Satpati, S. R. Biswas, P. P. Ray and B. Dey, *Langmuir*, 2023, **39**, 7469–7483.

30 D. J. Sutton, P. B. Tchounwou, N. Ninashvili and E. Shen, *Int. J. Mol. Sci.*, 2002, **3**, 965–984.

31 I. L. Steffensen, O. J. Mesna, E. Andruchow, E. Namork, K. Hylland and R. A. Andersen, *Gen. Pharmacol.*, 1994, **25**, 1621–1633.

32 K. Tanaka and T. Yoshimura, *New J. Chem.*, 2012, **36**, 1439–1441.

33 N. Spernovasilis, M. Psichogiou and G. Poulakou, *Curr. Opin. Infect Dis.*, 2021, **34**, 72–79.

34 M. M. Brown and A. R. Horswill, *PLoS Pathog.*, 2020, **16**, e1009026.